LA-UR-21-30426
Approved for public release; distribution is unlimited.

Title: Modeling soot growth in Comp-B using a detonation history

Author(s): Chang, Chong

Intended for: Report

Issued: 2021-10-20

September 16, 2021

Modeling soot growth in Comp-B using a detonation history

C. H. Chang

Los Alamos National Laboratory

A chemical kinetics procedure for soot formation calculation is summarized. By importing Lagrangian hydrodynamic calculations, species history is consistently accounted for. Detonation product composition is assumed in region with the burnt high explosive (HE). Soot formation is calculated using the density and energy obtained in the hydrodynamics calculation of HE detonation. Ideal gas equation-of-state (EOS) with temperature-dependent specific heat is used in the HE product region. Sample calculations show reasonably-expected temperature and soot formation.

I. INTRODUCTION

Soot formation during detonation of HE is composed of a number of complex physical and chemical processes including hydrodynamics, turbulence, chemical reactionss, and phase change. Conventional detonation modeling approaches do not usually involve all necessary modeling elements. For example, popular detonation calculation approaches based on the "reactive" burn models are employing the one step reaction approaches with EOS specially designed to produce the Chapman-Jouguet (CJ) condition. Needless to say, evolution of chemical species is not tracked in this approach. Furthermore, EOS used in these approaches such as Jones-Wilkins-Lee (JWL) seldomly produces accurate temperature.

There is a growing needs for studying chemical composition in more detail including soot formation during HE detonation. Modeling soot formation requires a number of capabilities which are not usually employed in detonation modeling. They include the lack of the reaction chains involving soot for the HE of interest. These chains describe evolution of a number of chemical species in the HE product. Soot formation and growth should also be a part of the reaction chain. All chemical reactions, in both HE burn and soot growth, are relatively slow compared to the hydrodynamic time scale, and thus species composition cannot be determined by the equilibrium composition. That is, it is necessary to model the species evolution using chemical kinetics, where the history of the species evolution must to be tracked.

Chemical reaction rates are commonly given in the Arrhenius form, in which the rates are expressed as functions of the temperature. Needless to say, correct calculation of temperature must be accompanied by the chemical kinetics. This requires the accurate representation of the "real gas" effects due to the elevated temperatures involved. Real gas effects are commonly represented in the temperature-dependent specific heats in the NIST data base. Unfortunately, the real gas effect is not included in JWL, and thus the temperature produced by JWL is not useful. Furthermore, it is common to employ a specialized JWL for each detonation model. That is, EOS depends on the flow and model.

In short, typical detonation calculations do not provide necessary information of temperature and chemical species evolution. Including the chemical kinetics of the reaction chain and thermodynamically accurate EOS has recently begun in solid HE burning such as HMX [1, 2]. Unfortunately, this effort is in its infancy, and it is not yet developed for Comp-B.

It is therefore necessary to establish a procedure to estimate soot formation and growth starting from the hydrodynamic simulation of solid HE detonation without chemical kinetics. The results

are imported into a chemical kinetics code, GRUS, in which temperature of each computational zone is calculated using the EOS with the real-gas effect. The chemical composition of the detonation product is set according to the known detonation product composition, from which chemical kinetics of the soot growth is calculated.

In this report, we present this approach for modeling soot formation and growth. The present approach is composed of three parts: (1) Reading and constructing history information, (2) calculation of temperature history using equation-of-state (EOS), and (3) chemical kinetics of soot formation and growth. Note that the history of the high explosive (HE) burning from the employed HE modeling code does not provide the evolution of species.

II. SUMMARY OF THE PROCEDURE

1. Read the input deck which contains the name of the record file, initial density, criteria for detonation, reaction rates, EOS information, and number of zones.

2. From the history file, read the current cycle information such as the time t, the lower zone boundary x_z, velocity (u_z) at x_z, density ρ_z, internal energy e_z, and pressure p_z. Subscript z is the zone index.

3. Determine zone information such as volume of the zone.

4. Determine if each zone contains detonation product or unburned HE, according to the criteria given in the input deck. Set species densities ρ_z^i in each zones. Species densities in the zones containing the detonation product are set only once when the zone becomes a detonation zone. Afterwards, soot densities evolve with the chemical kinetics.

5. Using EOS, determine p_z and T_z from ρ_z, ρ_z^i, and e_z.

6. Calculate carbon clustering evolution (soot growth) using the chemical kinetics based on T_z.

7. Start the next cycle, repeating from Step 2, until the end of the recored file is encountered.

Note that the employed hydro code needs to use the Lagrangian hydro scheme in order to have a consistent history in species density and energy. If Eulerian scheme is used, their histories involve advection (convection) from/to neighboring zones. Therefore, it becomes necessary to include convection of a large number of quantities in the present procedure. This effort is a large fraction of writing a reacting flow code, and the present procedure's fidelity would not be worth the effort. (It would be far better to implement the EOS and chemical kinetics into the hydro code.)

The thermodynamic quantities ρ, p, and e are located at the zone center, while velocity $\mathbf{u}$ is located at the zone boundary. The zone center and boundary locations are shown in Fig 1. Zone center is denoted by y_z. We have

$$y_z = \frac{x_z + x_{z+1}}{2} \tag{1}$$

$$V_z = \frac{4\pi}{3}\left(x_{z+1}^3 - x_z^3\right) \tag{2}$$

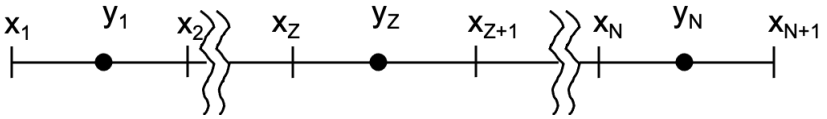

FIG. 1. Zone center and boundaries.

III. CHEMICAL KINETICS OF SOOT GROWTH

Evolution of chemical species can be calculated using the generalized chemical kinetics method proposed by Ramshaw and Chang [3]. Note that this routine calculates the change in internal energy due to the reaction energy release. However, it is unnecessary to track this energy change, since the energy history is already given. The temperature is obtained from ρ and e in the history.

Decomposition reaction of Comp-B is given by [4]

$$C_{4.58}H_{5.61}N_{4.82}O_6 \rightarrow 2.41N_2 + 2.24H_2O + 1.88CO_2 + 0.25CH_4 + 0.064H_2 + 2.45C$$

Carbon clustering reactions have been adopted from Ref. [5]. Carbon clusters are grouped into A_i, where A_i is the carbon cluster with $7i-1 \leq N_i^C \leq 7i+1$, where N_i^C is the number of carbons in A_i. The most common A_1 is the cluster with seven C atoms, and subsequent growth of soot is modeled as the agglomeration of these clusters. The reaction chain for the soot growth is then given by

$$A_1 + A_1 \stackrel{k_1}{\rightarrow} A_2$$
$$A_2 + A_1 \stackrel{k_2}{\rightarrow} A_3$$
$$A_3 + A_1 \stackrel{k_3}{\rightarrow} A_4$$

where k_s is the reaction rate. Note that all reactions involve A_1, implying that collisions between $A_{i>1}$ and $A_{i>1}$ are negligible. Reactions involving $A_{i>4}$ are ignored, and the first three reactions are included.

We solve the coupled differential equations (chemical kinetics) given by

$$\frac{dc_1}{dt} = -\sum_{i=1}^{3} k_i c_i c_1 \tag{3}$$
$$\frac{dc_2}{dt} = k_1 c_1 c_1 - k_2 c_2 c_1 \tag{4}$$
$$\frac{dc_3}{dt} = k_2 c_2 c_1 - k_3 c_3 c_1 \tag{5}$$
$$\frac{dc_4}{dt} = k_3 c_3 c_1 \tag{6}$$

where c_i is the molar concentration of A_i. The factor of half has been included in k_1. Note that the mass is conserved in the above equations.

For carbon cluster growth rates, we assume a typical Arrhenius reaction rate form given by

$$k_s = P_s \exp\left(-\frac{\Delta E_s + p\Delta V_s}{R_g T}\right) \tag{7}$$

where R_g=8.314 J/(mol K) is the universal gas constant, P_s is the frequency factor, ΔE_s is the activation energy, p is the pressure in bar, and ΔV_s is the activation volume. ΔV_s are calculated

reaction	1	2.	3
P_s (m^3/(mol*sec))	2.09920	13.2085	61.5800
ΔE_s (J/mol)	8.286×10^{-12}	0.0	0.0
ΔV_s (m^3/mol)	1.29657	1.20532	1.3072

TABLE 1: Values of C_i, D_i, and F_i.

as the specific volume difference between the current and initial conditions. Using the values presented in Ref. [5], values of P_s, ΔE_s, and ΔV_s are obtained by minimizing the $\sum_n \chi_n^2$, where $\chi_n = k_s^n - k_{ts}^n$, where k_{ts} are the values in the Table 6 of Ref. [5], and n is the index for the table entry for each reaction s. Values of P_s, ΔE_s, and ΔV_s are given in Table 1. Values of $\sum_n \chi_n^2$ for reactions i respectively are 9.847×10^{-6}, 4.3993×10^{-4}, and 3.62385×10^{-3}

IV. DETERMINATION OF DETONATED REGION

Detonation is not likely to be resolved in the history. We thus introduce assumptions:

- HE decomposition is very fast. Decomposition completes within a very short distance from the detonation wave.
- Evolution of carbon is a slow process.
- The effect of soot growth on the detonation temperature is negligible.
- Once burnt, composition of the HE product does not change except for the clustered carbon.

The whole HE region are subdivided into two regions: burnt and unburnt regions. The history of e_i, ρ_i, and/or p_i can be used in the criterion. For example, when a zone experiences a non-negligible increase in e_i, it would become a zone in the burnt region, and it would continue to be in the burnt region. Unburned zones are assumed to be occupied by the unburned HE, e.g., Comp-B. When a zone becomes a detonation zone for the first time, it is assumed to be occupied by the detonation product. Species concentrations are determined using the stoichiometric coefficients of the burning reaction. C is assumed to take the form of C_7. For example, 2.45 C in the decomposition of Comp-B becomes 0.35 C_7. A_i in burnt region (zones) then evolve using the chemical kinetics.

V. EOS USING THERMOCHEMICAL DATA

It is likely that the HE burning is modeled in the hydrodynamics code using the EOS tuned for the employed one-step reaction detonation model. JWL EOS has been popular in this approach. Unfortunately, JWL EOS is based on $p = (\gamma - 1)\rho e$ with a constant γ, the specific heat ratio. (p is the pressure.) If p is available instead of e, e can be determined using this relationship. In order to perform chemical kinetics calculations, accurate temperature T is necessary, but T from JWL EOS is seldomly accurate.

It is necessary to have EOS with correct e-T relationship. This is achieved by using the thermochemical data for each species which are available at the NIST website (https://webbook.nist.gov) and JANAF thermochemical data. Note that p in the JANAF-NIST EOS is determined from the ideal gas law. The dense gas effect around the detonation may need to be addressed.

Species	T(K)	A	B	C	D	E	F	H	$\Delta_f H$
N_2	100–500	28.98641	1.853978	-9.647459	16.63537	0.000117	-8.671914	0.0	0
	500–2000	19.50583	19.88705	-8.598535	1.369784	0.527601	-4.935202	0.0	
	2000–6000	35.51782	1.128728	-0.196103	0.014662	-4.553760	-18.97091	0.0	
H_2O	500–1700	30.09200	6.832514	6.793435	-2.534480	0.082139	-250.8810	-241.8264	-241.83
	1700–6000	41.96426	8.622053	-1.499780	0.098119	-11.15764	-272.1797	-241.8264	
CO_2	298–1200	24.99735	55.18696	-33.69137	7.948387	-0.136638	-403.6075	-393.5224	-393.51
	1200–6000	58.16639	2.720074	-0.492289	0.038844	-6.447293	-425.9186	-393.5224	
CH_4	298–1300	-0.703029	108.4773	-42.52157	5.862788	0.678565	-76.84376	-74.87310	-74.87
	1300–6000	85.81217	11.26467	-2.114146	0.138190	-26.42221	-153.5327	-74.87310	
H_2	298–1000	33.066178	-11.363417	11.432816	-2.772874	-0.158558	-9.980797	0.0	0
	1000–2500	18.563083	12.257357	-2.859786	0.268238	1.977990	-1.147438	0.0	
	2500-6000	43.413560	-4.293079	1.272428	-0.096876	-20.533862	-38.515158	0.0	
C	298-6000	21.17510	-0.812428	0.448537	-0.043256	-0.013103	710.3470	716.6690	716.67

TABLE 2: Values of the coefficients of gas species.

Burning HE is composed of many species, and EOS would depend on the species composition. Due to the dynamic situation of chemical kinetics, it is impossible to create a mixture EOS, since the species composition is not known a priori. Therefore, we plan to construct the EOS using the mixture rule and the species composition results from the chemical kinetics. Using the mixture rule will involve equilibration of p and T that is obtained by the iteration technique presented in this section.

V.1. Specific heats and enthalpies

Comp-B is composed of 60 % RDX ad 40 % TNT. Paraffin wax binder is ignored in EOS. Both RDX and TNT can be assumed to exist only as solids. Its detonation product are N_2, H_2O, CO_2, CH_4, H_2, and C. C is assumed to take the condensed phase, while the others are in gas phase.

For gas species, the constant pressure specific heats, C_p are given by

$$C_p = A + Bt + Ct^2 + Dt^3 + \frac{E}{t^2} \qquad \text{(J/(mol K))} \tag{8}$$

where $t = T/1000.0$ is the scaled temperature. Specific enthalpy is given by

$$h - h_{298.15} = At + \frac{1}{2}Bt^2 + \frac{1}{3}Ct^3 + \frac{1}{4}Dt^4 - \frac{E}{t} + F - H \qquad \text{(kJ/mol)} \tag{9}$$

Note the difference in units. Coefficients are given in Table 2. Constant volume specific heats, C_v, of gases are given by $C_v = C_p - R_g$ J/(mol K)), where $R_g = 8.3145$ J/(mol K) is the universal gas constant. For condensed phases, R_g is not subtracted from C_p for simplicity. $\Delta_f H$ are in kJ/mol.

The internal energy is given by

$$e = \int_{t_{ref}}^{t} C_v dt \tag{10}$$

where t_{ref} is the reference temperature. ($T_{ref} = 298.15$ K, $t_{ref} = 0.29815$). The corresponding temperature can be obtained by solving this equation, which usually involves iterations.

Species	T(K)	C_p (J/(mol K))	$\Delta_f H$ (kJ/mol)
C	300-1800	10.68	0
RDX	200–475	248.9	79.1
TNT	290–345	243.3	-63.2

TABLE 3: Values of the coefficients for condensed phases. $\Delta_f H$ for C is for graphite.

In our modeling, carbon compounds A_1, A_2, A_3, and A_4 are involved. They are respectively composed of approximately 7, 14, 21, and 28 carbon atoms. Thermophysical data are not available for them. We thus use the data for condensed carbon atoms in Tables 2 and 3. However, these values are expected to produce significant error due to the large difference in the atomic weight. This dilemma is circumvented by multiplying the mass ratio to the data, e.g., $C_p^{A_1} = 7C_p^C$, etc. This way, temperature would not change by the soot formation. C_p and $\Delta_f H$ of condensed C, RDX, and TNT are listed in Table 3.

Since the detonation temperature of most HE is lower than the sublimation temperature of carbon (about 4000 K), the carbon in the HE product is expected be in condensed phase, taking the form of single atom or a cluster of small number of atoms. It thus appears to be correct to use the thermophysical properties in Table 3. Gas phase carbon can be ignored for the current purpose. Note that it is necessary to treat gas phase carbon as different species from the solid state carbon when gas phase carbon is included in the model. Condensation reaction can then be treated as a chemical reaction, with heat of reactions determined using $\Delta_f H$ of the C in condensed and gas phases.

V.2. Pressures

It is necessary to calculate pressure of each species. Pressure is obtained using the ideal gas law as

$$p = \rho \frac{R_g}{M} T \tag{11}$$

where ρ is the density, and M is the molecular weight. For condensed phases, pressure is not calculated. (This is consistent with $\gamma = 1$ used for condensed phases, where γ is the specific heat ratio.). To control the pressure calculation, a new input variable for each species, T_{cut}^p, variable is introduced. Material pressure is calculated when $T > T_{cut}^p$. By setting T_{cut}^p as a reasonably large value, pressure calculation can be avoided.

V.3. Mixture

EOS is given for each species. In a mixture, it is then necessary to obtain common temperature and pressure from the given mixture density and energy (or temperature and energy from density and pressure). For this purpose, we use Amagat's law in which each species are assumed to be segregated, occupying its own subvolume. Pressure of condensed phase is ignored. Subscript i denotes the species i, y_i is the mass fraction of species i, the specific volume is $v_i = 1/\rho_i$.

Thermodynamic quantities are related as

$$\rho = \sum_i \alpha_i \rho_i \tag{12}$$

$$e = \sum_i y_i e_i \tag{13}$$

$$y_i = \frac{\alpha_i \rho_i}{\rho} \tag{14}$$

$$\alpha_i = \rho y_i v_i \tag{15}$$

where α_i is the volume fraction of species i. When multiple materials are present, α_i is the relative species volume fractions in each material, not the species volume fraction of the whole computational zone. Therefore, $\sum_i \alpha_i$ is always unity. Note that the material index has been omitted, and the iteration procedure below is used for each material.

V.4. T and p from ρ and e

The temperature and pressure of each species must be obtained using the species EOS in such a way that the resulting T_i and p_i of each species i are identical, and the common T and p respectively become the material temperature and pressure. The species volume fractions are adjusted so that p_i becomes identical. The host code provides the internal energy e and species mass fractions y_i and the mixture density ρ, thus our objective is to find e_i satisfying $T_i = T$ and $p_i = p$ from the given e, ρ, and y_i.

Changes in pressure and temperature are given by

$$\Delta p_i = p^{\nu+1} - p_i^{\nu} = \left(\frac{\partial p}{\partial v}\right)_e^i \Delta v_i + \left(\frac{\partial p}{\partial e}\right)_v^i \Delta e_i \tag{16}$$

$$\Delta T_i = T^{\nu+1} - T_i^{\nu} = \left(\frac{\partial T}{\partial v}\right)_e^i \Delta v_i + \left(\frac{\partial T}{\partial e}\right)_v^i \Delta e_i \tag{17}$$

Note that $p^{\nu+1}$ and $T^{\nu+1}$ is used for $p_i^{\nu+1}$ and $T_i^{\nu+1}$ in Eqs. (16) and (17), since our objective is to obtain $p = p_i$ and $T = T_i$ at iteration $\nu + 1$. Changes in v_i and e_i are then given by

$$\Delta v_i = \frac{A_i^4 \Delta p_i - A_i^2 \Delta T_i}{A_i^1 A_i^4 - A_i^2 A_i^3} \tag{18}$$

$$\Delta e_i = \frac{A_i^1 \Delta T_i - A_i^3 \Delta p_i}{A_i^1 A_i^4 - A_i^2 A_i^3} \tag{19}$$

where $A_i^1 = (\partial p/\partial v)_e^i$, $A_i^2 = (\partial p/\partial e)_v^i$, $A_i^3 = (\partial T/\partial v)_e^i$, and $A_i^4 = (\partial T/\partial e)_v^i$. In our model based on ideal gas, we have

$$A_i^1 = -\frac{R_i T_i}{v_i^2} \tag{20}$$

$$A_i^2 = \frac{R_i}{C_{vi} v_i} \tag{21}$$

$$A_i^3 = 0 \tag{22}$$

$$A_i^4 = \frac{1}{C_{vi}} = \frac{1}{C_{pi} - R_i} \tag{23}$$

where $R_i = R_g/M_i$ is the gas constant of species i.

In a mixture, Δv_i and Δe_i satisfy

$$\sum_i y_i \Delta v_i = 0 \tag{24}$$

$$\sum_i y_i \Delta e_i = 0 \tag{25}$$

Combining Eqs. (16), (17), (24), and (25), we have

$$\sum_i B_i A_i^4 \left(p^{\nu+1} - p_i^\nu\right) - \sum_i B_i A_i^2 \left(T^{\nu+1} - T_i^\nu\right) = 0 \tag{26}$$

$$\sum_i B_i A_i^1 \left(T^{\nu+1} - T_i^\nu\right) - \sum_i B_i A_i^3 \left(p^{\nu+1} - p_i^\nu\right) = 0 \tag{27}$$

where

$$B_i = \frac{y_i}{A_i^1 A_i^4 - A_i^2 A_i^3} \tag{28}$$

The material pressure p and temperature T are determined from Eqs. (26) and (27).

The Newton iteration procedure is summarized as

1. Make an initial guess. We typically use $e_i = e$, $v_i = 1/\rho$, $p^\nu = \rho \sum_i y_i v_i p_i$ and $T^\nu = (1/N) \sum_i T_i$, where N is the number of species present. Species EOS is used in obtaining p_i and T_i.

2. Evaluate T_i^ν, p_i^ν, A_i^1, A_i^2,A_i^3, A_i^4, and B_i, using the EOS table for species i. Since T and v are the grid variables in the EOS tables used, we approximate $A_i^3 = 0$, which does not seem to influence the convergence of this iteration.

3. Obtain $p^{\nu+1}$ and $T^{\nu+1}$ using Eqs. (26) and (27).

4. Test convergence by comparing $p^{\nu+1}$ and $T^{\nu+1}$ with p^ν and T^ν.

5. If not converged, evaluate Δv_i and Δe_i, using Eqs. (18), and (19). Under-relaxation can be used by multiplying the relaxation factors to Δv_i and Δe_i.

6. Set $p_i^\nu = p^{\nu+1}$ and $T_i^\nu = T^{\nu+1}$, and repeat the procedure until convergence.

The procedure described here employs an efficient 2×2 system.

V.5. When solid species is present

Iteration procedure above can still be used when a condensed phase species is present. When an adequate pressure and associated derivatives are not provided by the species EOS, we can set its pressure as $p^{\nu+1}$ during the iteration. We can use $(\partial p/\partial e)_v^i = 0$. The stiffness can be represented by approximating $(\partial p/\partial v)_e^i$ as a large negative value.

V.6. T and e from ρ and p

Since a Lagrangian hydro code provides the equilibrated pressure p, we can adopt another approach, taking advantage of $\Delta p_i = 0$. We start from

$$\Delta T_i = T^{\nu+1} - T_i^{\nu} = \left(\frac{\partial T}{\partial v}\right)_p^i \Delta v_i + \left(\frac{\partial T}{\partial p}\right)_v^i \Delta p_i = \left(\frac{\partial T}{\partial v}\right)_p^i \Delta v_i \tag{29}$$

For ideal gas, we have $(\partial T/\partial v)_p^i = C_i = p_i/R_i$. We also have

$$\sum_i y_i \Delta v_i = \sum_i \frac{y_i}{C_i} \Delta T_i = 0 \tag{30}$$

The iteration procedure is summarized as

1. Make the initial guess of $v_i = 1/\rho$ and $T^{\nu} = (1/N)\sum_i T_i$, where N is the number of species present. T_i obtained from the EOS for species i using the given p and y_i.
2. Obtain $T^{\nu+1}$ using Eq. (30).
3. Test convergence by comparing $T^{\nu+1}$ with T^{ν}.
4. If not converged, evaluate Δv_i, using Eq. (29). (C_i is known.) Under-relaxation can be used by multiplying the relaxation factors to Δv_i.
5. Set $T_i^{\nu} = T^{\nu+1}$, and repeat the procedure until convergence.
6. When converged, obtain e_i from T_i using species EOS.

When solid species is present, they are excluded in the Steps 2 and 4, i.e., in evaluating Δv_i and $\sum_i y_i/C_i$. In practice, the approach of obtaining T and p from ρ and e seems to produce more reasonable results.

V.7. HMX

Due to the large oxygen content, soot formation is usually neglected in HMX burning. An approximated stoichiometry of HMX burning involving soot formation is given by [6]

$$C_4H_8N_8O_8 \rightarrow 2\ N_2 + 4H_2O + 2CO_2 + 2C$$

HMX properties are given by $C_p = 290.2$ J/(mol K) at 298 K, $\Delta_f H = 74.9$ KJ/mol. Note that the accuracy of the stoichiometry above is questionable. A reliable stoichiometry will be reported when found.

VI. TEST CALCULATION RESULTS

The present procedure has been applied to a Comp-B bare charge problem. HE detonation has been calculated by a Lagrangian hydro code. Simulation has been carried out in 1-D spherical domain. The Comp-B radius R are 5, 10, 15, 20, 25, 30, 35, 40, 45 and 50 cm. Comp-B explodes

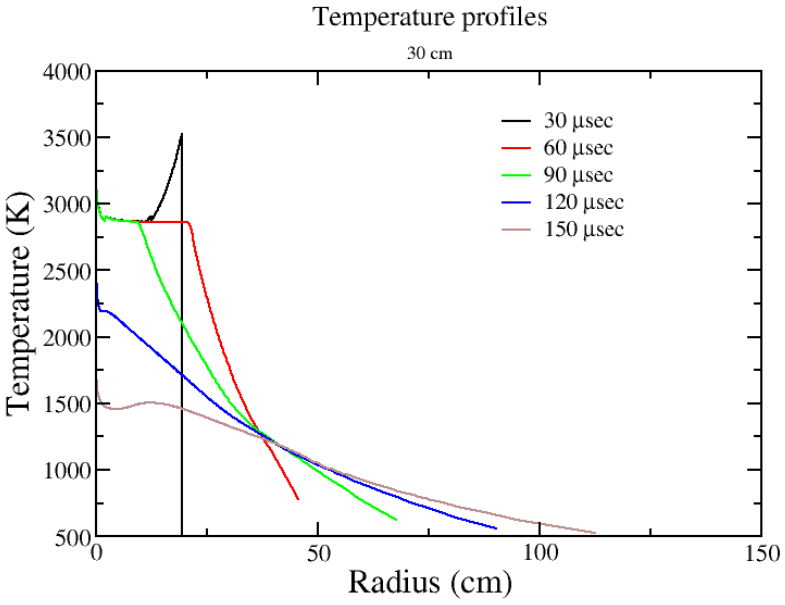

FIG. 2. Evolution of temperature of the 30 cm case.

then expands into vacuum. The initial mesh size is 0.1 cm for all cases. Calculations ran to $5R$ μsec. E.g., 30 cm case ran to 150 μsec.

Temperature evolution of the 30 cm case is shown in Fig. 2. Detonation wave is shown at 30 μsec, and the others temperature profiles show typical behavior in expansion into vacuum. Note that the peak temperature of the detonation wave is much lower than typical temperatures obtained using the one-step reactive burn model with corresponding JWL, which usually is higher than the adiabatic flame temperature, which is unphysical. The advantages are obvious of our EOS approach based on the real gas effects.

Concentration evolutions of A_i at the corresponding times are shown in Fig. 3. Again, detonation wave location is shown in Fig. 3a. Needless to say, until detonation wave arrives, soot is not formed. As HE burning and expansion progress, the peak values of A_1 concentration decreases due to the spread associated with the HE product expansion. Note also that A_1 is consumed by the growth of larger carbon clusters $A_{i\geq 2}$. In particular, A_4 concentration becomes larger than $A_{2,3}$ concentrations, indicating substantial growth of A_4. Observe that formation and growth are ignored for $A_{i>4}$, implying that A_4 represent all carbon clusters $A_{i\geq 4}$. We expect that including formation and growth reactions for $A_{i\geq 4}$ would reduce A_4 concentration to smaller values than A_3 concentration. ($A_{i\geq 5}$ would of course be added to Fig. 3.)

Figure 4 shows temperature profiles of all cases at the end of calculations. It appears that the relative magnitudes of the calculation run times are adequately set for varying HE size, as the temperature profiles are similar. If lower temperatures need to be produced, calculation run times should obviously be increased.

Figure 5 shows A_i concentration profiles at the end of calculations for 5, 30, and 50 cm cases. Observe that A_i profiles are not similar as the temperature profiles shown in Fig. 4. Furthermore, concentrations of $A_{i>1}$ in the 30 and 50 cm cases are much larger than the 5 cm case. The time for carbon clustering or soot growth is larger in the larger charge cases, producing larger cluster sizes. Needless to say, correct modeling of carbon clustering requires chemical kinetics accompanied by

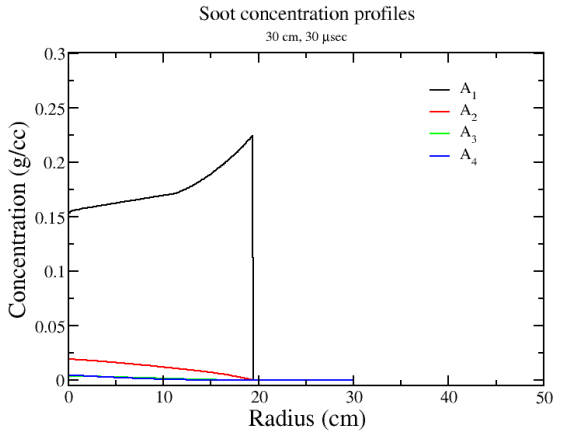

(a) At 30 μsec

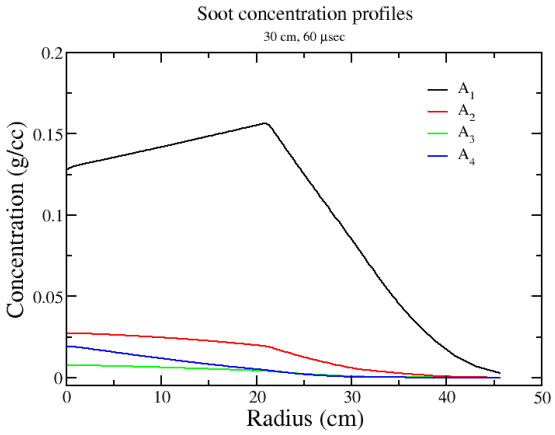

(b) At 60 μsec

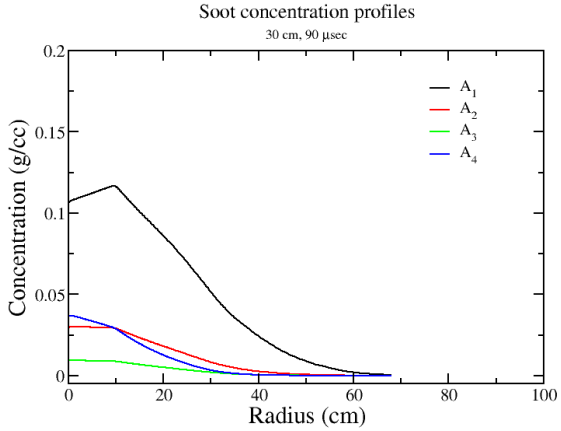

(c) At 90 μsec

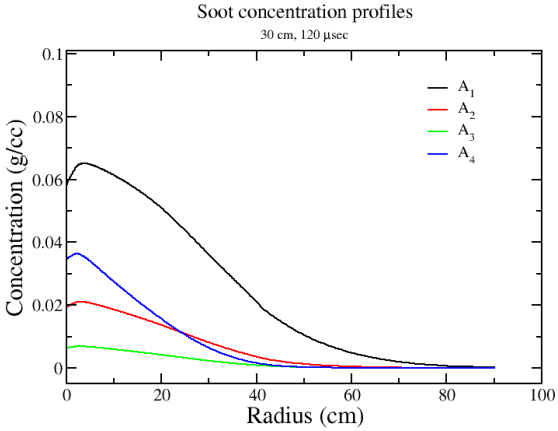

(d) At 120 μsec

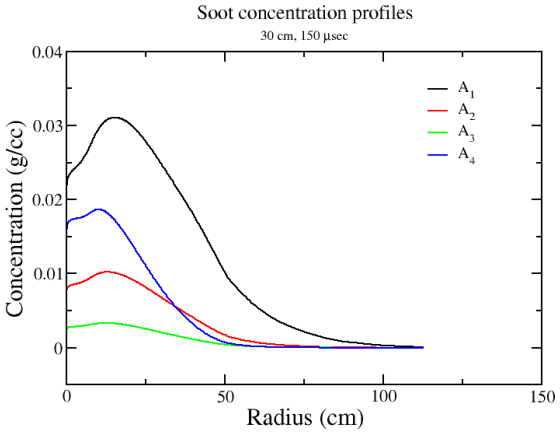

(e) At 150 μsec

FIG. 3. Evolution of the A_i concentration of the 30 cm case.

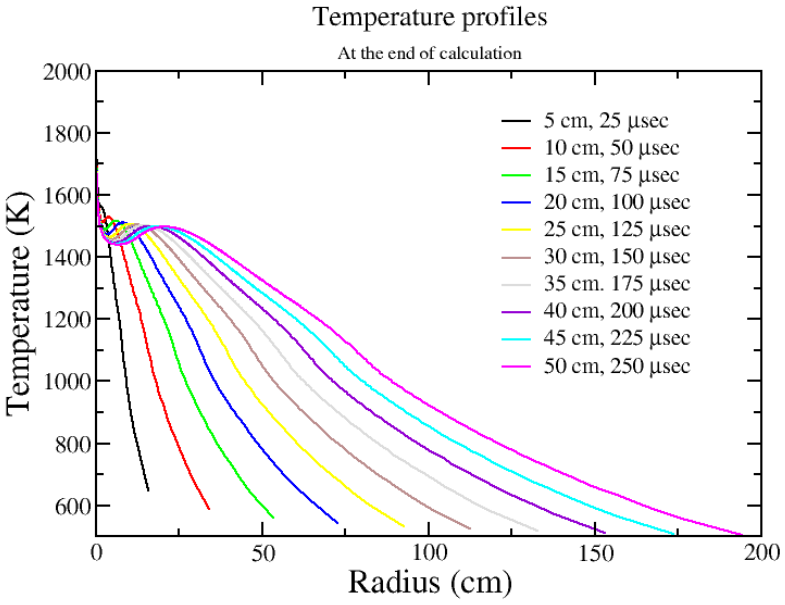

FIG. 4. Temperature profiles at the end of calculation.

realistic EOS.

Simulations of the soot formation from the burning of comp-B sphere of identical sizes have also been carried out with air placed outside of the HE sphere. The mass of air was set ten times the Comp-B mass. Although the air still expands into vacuum at the outer boundary, the HE burning calculations finish before the expansion arrives at the HE. Since HE expansion encounters the stationary air with a large amount of inertia, HE product is compressed at the boundary which are shown in the figures below. Figures 6–9 show similar results as the cases of HE product expansion into vacuum shown in Figs. 2–5. Main differences are (1) the expansion is slower since the HE product is pushing out air, and (2) compression occurs at the HE-air interface.

VII. REMARKS

Calculation procedure for soot formation and growth has been presented. Hydrodynamic calculation of HE detonation is carried out by a Lagrangian hydrodynamics code, providing mesh evolution, density, and energy. Chemical composition of the detonation product, including carbon, also needs to be provided. The temperature is then calculated using the ideal gas EOS with real gas effects, and chemical kinetics of soot growth is calculated using this temperature. It appears that reasonable results for temperature evolution and soot growth are produced.

Note that HE product composition is assumed to be the detonation product. This could become a source of error when detonation is no longer the HE burning mechanism. Another source of error is the use of the ideal gas EOS. The real gas effect only incorporates the temperature-dependent specific heat which is important for the correct' modeling at the elevated temperature. However, the dense-gas effect is not included, and it could lead to errors when the density is very high such as where detonation takes place.

The present procedure may provide useful information in the absence of a fully integrated

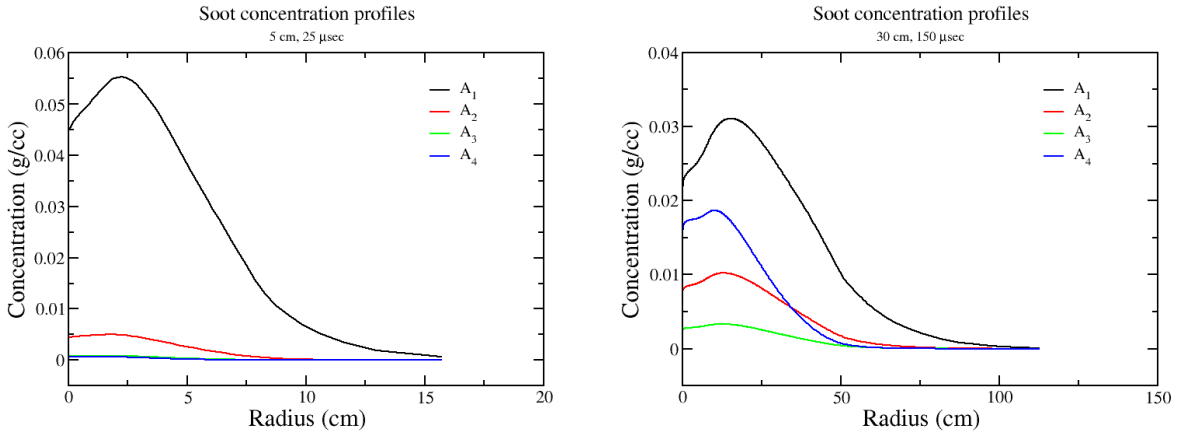

(a) 5 cm charge at 25 μsec

(b) 30 cm charge at 150 μsec

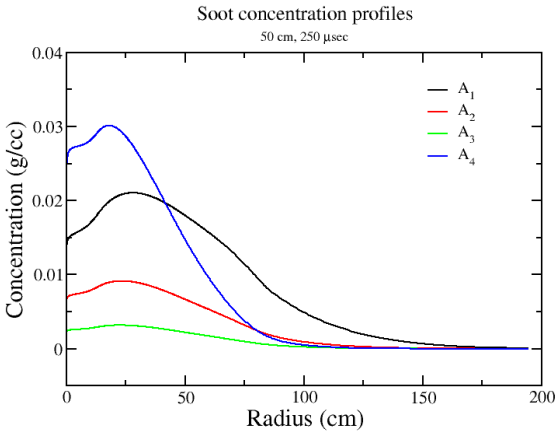

(c) 50 cm charge at 250 μsec

FIG. 5. A_i concentration profiles of 5, 30 , and 50 cm cases at the end of calculation.

computational tool. However, it may eventually become necessary to include the chemical kinetics and realistic EOS in the hydrodynamics simulation of HE burning as in Refs. [1, 2].

VIII. ACKNOWLEDGEMENT

I am grateful to Toru Aida for providing detonation calculation results.

[1] C. H. Chang and A. J. Scannapieco, *HMX detonation calculation using multi-reaction chain (Ver. 2)*, Report LA-UR-20-25658 (Los Alamos National Laboratory, 2020).

[2] C. H. Chang and A. J. Scannapieco, *Simulation of flame acceleration and deflagration-to-detonation transition with heat transfer in HE product and fractured HE*, report LA-UR-21-20155 (Los Alamos National Laboratory, 2021).

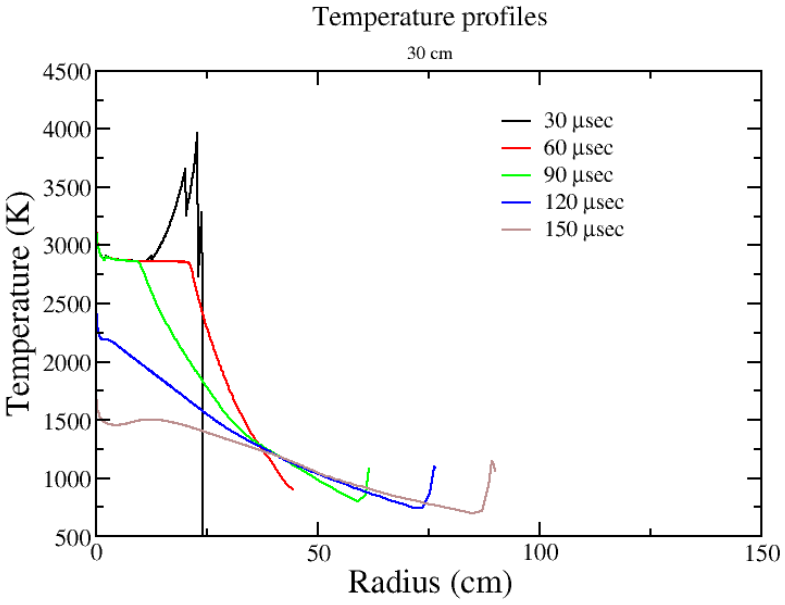

FIG. 6. Evolution of temperature of the 30 cm case with air.

[3] J. D. Ramshaw and C. H. Chang, "Iteration scheme for implicit calculations of kinetic and equilibrium chemical reactions in fluid dynamics," J. Comput. Phys. **116**, 359–364 (1995).

[4] M. L. Hobbs, M. J. Kaneshige, and M. U. Anderson, *Cookoff of a melt-castable explosive (Comp-B)*, Tech. Rep. SAND2012-10207C (Sandia National Laboratory, 2012).

[5] N. Rom, B Hirshberg, Y. Zeiri, D. Furman, S. Zybin, III W. A. Goddard, and R. Kosloff, "First-principlesbase reaction kinetics for decomposition of hot, dense liquid TNT from ReaxFF multiscale reactive dynamics simulations," J. Phys. Chem. C **117**, 21043–21054 (2013).

[6] M. S. Shaw and J. D. Johnson, "Carbon clustering in detonations," J. Appl. Phys. **62**, 2080–2085 (1987).

Appendix A: Test of chemical kinetics and EOS

The test problem used in Ref. [3] has been used to ensure the correct implementation of the chemical kinetics and EOS routines. Note that the temperature evolution has been simplified in the present procedure, producing slightly different temperature evolution. Calculation results are shown in Fig. 10.

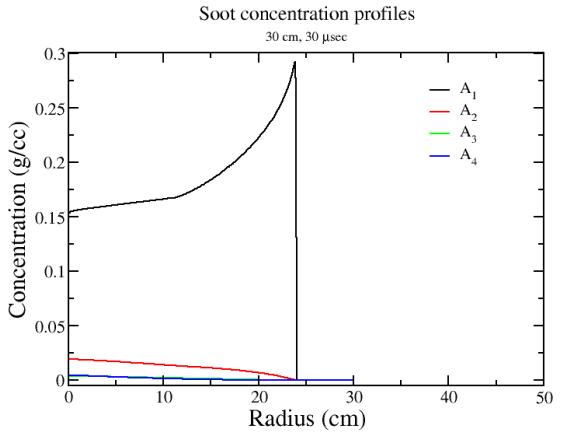

(a) At 30 μsec

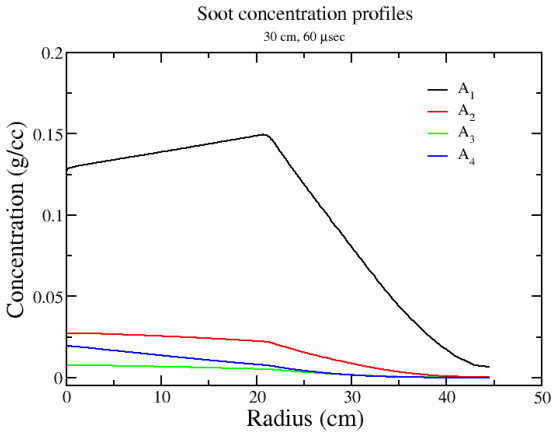

(b) At 60 μsec

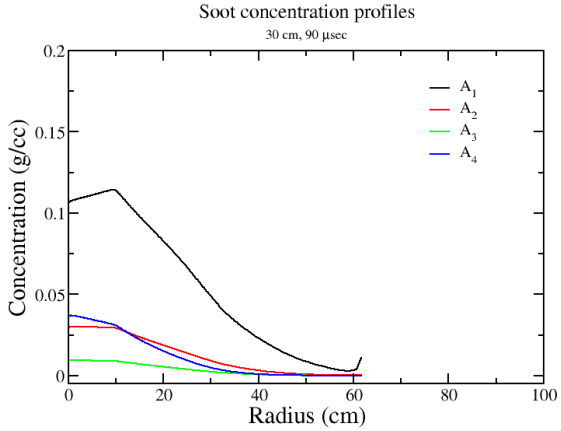

(c) At 90 μsec

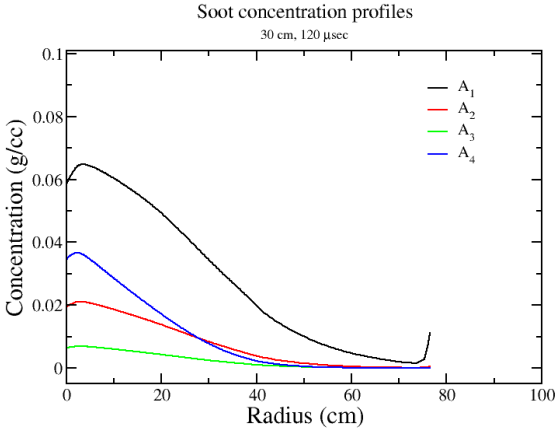

(d) At 120 μsec

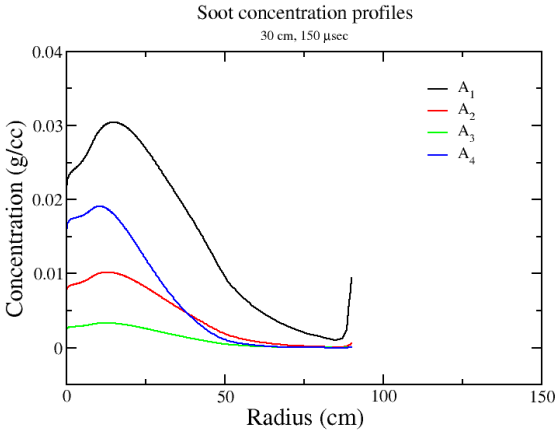

(e) At 150 μsec

FIG. 7. Evolution of the A_i concentration of the 30 cm case with air.

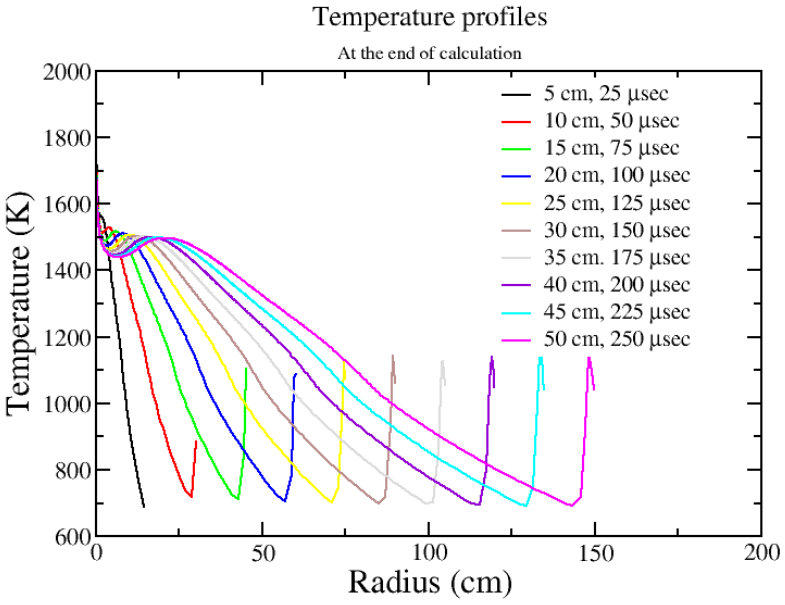

FIG. 8. Temperature profiles at the end of calculation with air.

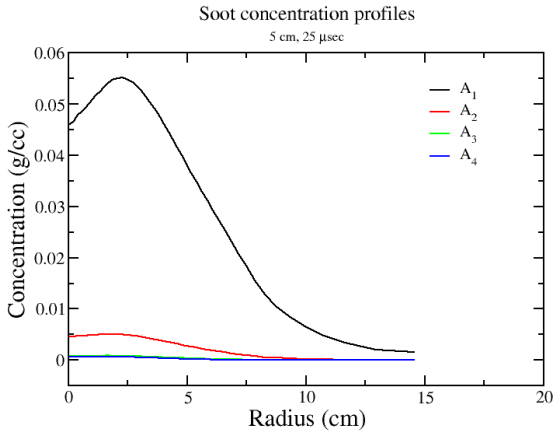

(a) 5 cm charge at 25 μsec

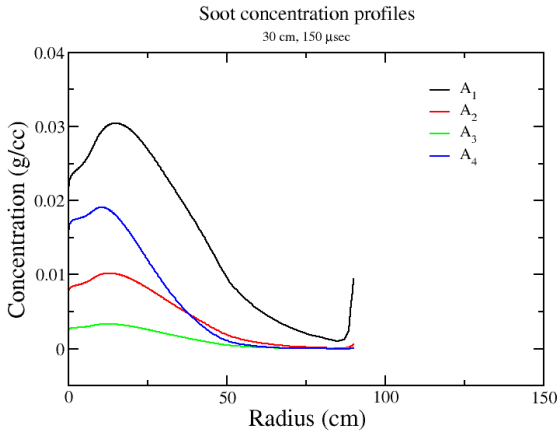

(b) 30 cm charge at 150 μsec

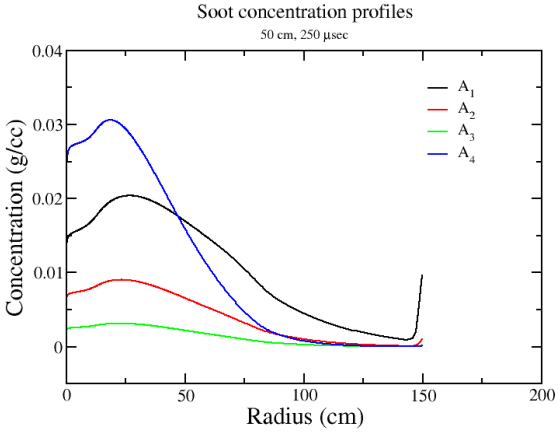

(c) 50 cm charge at 250 μsec

FIG. 9. A_i concentration profiles of 5, 30 , and 50 cm cases with air at the end of calculation.

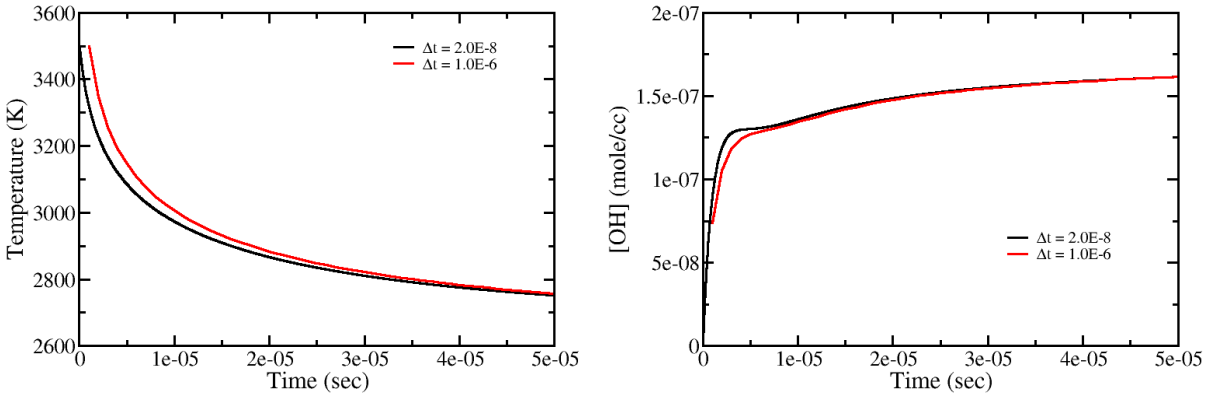

(a) Temperature

(b) Case1 at 3.08 μsec

FIG. 10. Evolution of temperature and [OH].